Journal of Power Sources 242 (2013) 157–165

Contents lists available at SciVerse ScienceDirect

Journal of Power Sources

journal homepage: www.elsevier.com/locate/jpowsour

Non-precious cathode electrocatalyst for magnesium air fuel cells: Activity and durability of iron-polyphthalocyanine absorbed on carbon black

Zhongfang Li*, Jianwei Yang, Guofeng Xu, Suwen Wang

School of Chemical Engineering, Shandong University of Technology, #12 Zhangzhou Road, Zibo, 255049 Shandong Province, PR China

HIGHLIGHTS

- A planar iron-polyphthalocyanine (PPcFe) with a large-area π bond is synthesized.
- PPcFe/C exhibits high oxygen reduction activity.
- Spectral and electrochemical studies show that PPcFe/C has excellent durability.
- A magnesium/PPcFe/C-air cell has excellent discharge performance and stability.

GRAPHICAL ABSTRACT

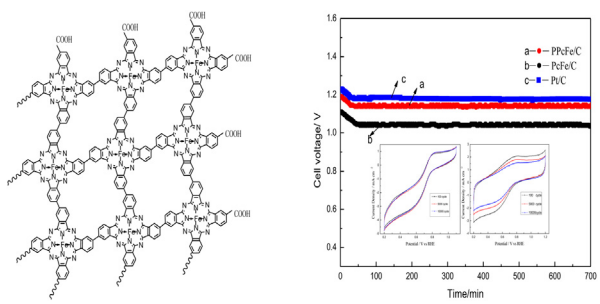

ARTICLE INFO

Article history:
Received 2 April 2013
Received in revised form
17 May 2013
Accepted 19 May 2013
Available online 28 May 2013

Keywords:
Magnesium air fuel cells
Air electrode
Catalyst
Oxygen reduction reaction
Iron polyphthalocyanine
Durability

ABSTRACT

A planar iron-polyphthalocyanine (PPcFe) oxygen reduction reaction (ORR) catalyst for magnesium air fuel cells (MAFC) is prepared by dispersing PPcFe on carbon black (C) and heating under argon. Thermogravimetric analysis shows PPcFe is stable below 600 °C. The X-ray diffraction and X-ray photoelectron spectroscopy results show the active site of PPcFe/C is the FeN_4 in the phthalocyanine ring. The rotating disk electrode measurements in 0.5 M L^{-1} H_2SO_4 solution show the initial potential for ORR is 0.82 V vs. RHE at 20 °C and that it mainly occurs via a four-electron process. Almost no performance degradation is observed over continuous cyclic voltammetry at 10,000 cycles, linear sweep voltammetry at 200 cycles, and 60 h of the chronoamperometry test. The infrared spectrum of PPcFe, after all the durability tests, shows no changes from the initial characteristics. The polarization curves of the air electrodes with PPcFe/C, iron-phthalocyanine/C and Pt/C catalysts exhibit excellent polarization performances. The discharge performance of a MAFC single cell with PPcFe/C cathode catalyst shows an open circuit potential of 1.74 V, with a peak power density of 50.5 mW cm^{-2} at 20 °C. The cell voltage decreases less than 0.01 V during continuing discharge @ 20 mA cm^{-2} for more than 11 h.

© 2013 Elsevier B.V. All rights reserved.

1. Introduction

Metal–air cells are fuel cells in which the "fuel" is a metal. They are promising power sources because of their high theoretical voltage, high specific energy, low cost, light weight, and environmental compatibility [1,2]. These cells generate electricity through the reaction between oxygen and metal sheets in a liquid electrolyte. Common metal anode sheets are magnesium [3], zinc [4], aluminum [5], and lithium [6]. Magnesium is known for its high theoretical specific charge capacity (2205 Ah kg^{-1}) [7], which makes it an excellent metal–air fuel cell anode candidate. Magnesium–air fuel cell (MAFC) performance is mainly influenced by

* Corresponding author. Tel./fax: +86 533 2786290.
E-mail addresses: zhfli@sdut.edu.cn, lizhongfangzb@126.com (Z. Li).

0378-7753/$ – see front matter © 2013 Elsevier B.V. All rights reserved.
http://dx.doi.org/10.1016/j.jpowsour.2013.05.082

the cathode. The cathode reaction of a metal–air fuel cell involves an oxygen reduction reaction (ORR) process. Thus, the electrocatalyst in the cathode is an important factor in determining cathode performance. ORR catalysts have been extensively studied for many years in the field of fuel cell technologies. The cathode catalyst largely determines the energy conversion efficiency and cost of a fuel cell stack [8–10]. Recent studies have utilized noble metal catalysts, such as platinum (Pt)-group metals [11–13] with high activity and excellent selectivity. However, the limited availability and high cost of these catalysts limit their extensive application. Several studies have focused on reducing Pt loading [14] and using non-noble metal electrocatalysts as a lower-cost alternative. Non-noble catalysts have received considerable attention for application as cathode ORR catalysts [15] especially in alkaline and neutral media, which become alkaline on discharge. These non-noble metal catalysts mainly include transition metal oxides, such as MnO_x, CoO_x, ZrO_x, and TiO_x [16–18], spinels, carbon-based metal-free materials [19,20], and metal–N–C cluster catalysts [21,22]. Spinel and transition metal-oxide catalysts are inexpensive and easy to prepare. However, their low activity makes these catalysts unsuitable for discharge at high currents. Furthermore, the $Mg(OH)_2$ precipitation at the cathode during MAFC operation negatively affects the air permeability of the cathode. This problem is typically solved by using an acid treatment.

Metal-oxide and spinel catalysts are not applicable to MAFCs because of their poor tolerance to acid. Carbon-based materials without doping have low ORR activity. However, nitrogen or sulfur doping of carbon-based materials can improve ORR catalytic activity [23,24]. Several studies have attempted to develop metal-free ORR catalysts [25–27]. Metal–N–C cluster catalysts mainly include polypyrrole [28], polyaniline [29], and transition metal macrocycles (TMMs). Polypyrrole and polyaniline transition metal Fe and Co composites have attracted considerable interest for application in fuel cells. These metal coordination compounds are converted into cluster after thermal treatment, which can improve ORR catalytic activity. Pyrolyzing mixtures of metallic salt, organic precursor, and ammonia in an inert atmosphere produce similar results [30,31]. TMMs [32–35], such as transition metal porphyrins and phthalocyanines, have been actively studied as promising ORR catalysts [36–39]. Several studies have revealed that pyrolyzed TMM catalysts are more active and stable than their unpyrolyzed analogs [40]. These catalysts are usually pyrolyzed at high temperatures (>700 °C), when they are converted to metal–N–C clusters. The nature of the active ORR sites that form during pyrolyzation remains debatable [41, 42]. The structure of these catalysts is yet to be satisfactorily defined to perform accurate quantitative studies. These catalysts show poor durability because of the loss of either unchelated metal or metal in a partially chelated catalyst structure [43]. The durability of these classes of catalysts therefore requires further study.

This study aims to develop ORR catalysts with high activity, selectivity, long lifetime, and excellent tolerance to acid. A planar iron-polyphthalocyanine (PPcFe) catalyst was designed. The molecular skeleton of the polymer forms continuous one pi (π) bond, such that the π electron delocalization energy increases and the capacity of the molecule for electron gain or loss improves. This type of catalyst is considered to have high activity and excellent durablility.

The resulting PPcFe/C was characterized using X-ray diffraction (XRD) and X-ray photoelectron spectroscopy (XPS). The electrocatalytic properties of this catalyst in 0.5 M L^{-1} H_2SO_4 solution were determined using a rotating disk electrode (RDE). Electrochemical and Fourier transform-infrared (FT-IR) spectroscopy analyses were performed to evaluate the catalytic and chemical stabilities under a strengthened fuel cell working environment. The air electrode was prepared, and the MAFC single cell was assembled and its performance was evaluated. The catalysis of MAFC using PPcFe/C was studied, which is of great practical significance. The experimental logic is schematically shown in Fig. 1.

2. Experimental

2.1. Preparation of PPcFe

The synthesis of Fe (II) –4, 4′, 4″, 4‴-phthalocyanine tetracarboxylic acid (TcPcFe) was based on a previously reported procedure [44]. UV–vis frequencies of TcPcFe in concentrated H_2SO_4 were: λ_{max}: 302 nm (B band), 779 nm (Q band); IR (KBr) ν:

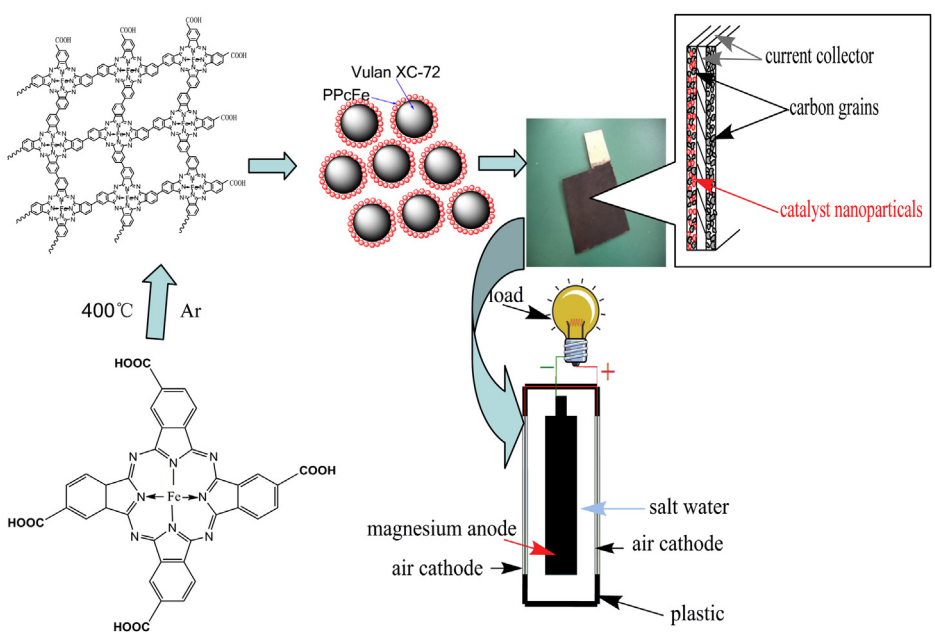

Fig. 1. The experimental logic.

750 cm^{-1}, 907 cm^{-1}, 1060 cm^{-1}, 1088 cm^{-1}, 1598 cm^{-1}, 1716 cm^{-1}, 1750 cm^{-1}, 3435 cm^{-1}.

Finely ground Fe (II)-4, 4′, 4″, 4‴-phthalocyanine tetracarboxylic acid (TcPcFe) was placed in a porcelain boat, which was then put into a homemade reactor and purged with argon (Ar) gas by repeated evacuation and refilling. The boat was then heated to 400 °C under Ar for 2 h. The resulting power was PPcFe. Frequencies under the same conditions as those above were: PPcFe: λ_{max}: 315 nm (B band), 774 nm (Q band); IR (KBr) ν: 749 cm^{-1}, 907 cm^{-1}, 1061 cm^{-1}, 1090 cm^{-1}, 1599 cm^{-1}, 1716 cm^{-1}, 1751 cm^{-1}, 3435 cm^{-1}. The structure of the PPcFe is shown in Fig. 2.

2.2. Preparation of PPcFe/C

PPcFe was adsorbed onto high surface area carbon black (C) powder (Vulcan XC-72; Cabot Corporation, Boston, MA) according to the following procedure. A total of 0.5 g of PPcFe was dispersed with 0.5 g of XC-72 in 40 mL of dimethyl sulfoxide (Aldrich, Milwaukee, WI). The dispersion was stirred under reflux, heated for 24 h, and dried at 75 °C under air for 12 h. Finally, the precipitate was ground into fine powder and subsequently heat treated under Ar at a temperature of 400 °C. A sample of the catalyst with PPcFe/C mass ratio was 1:1 (the FeN_4 loading is 7.5%). The catalysts are prepared with different ratios of PPcFe and C (1:1, 1:1.5, 1.5:1corresponding to 7.5%, 6%, 9% FeN_4 loading) and at different heat-treatment temperature (400 °C, 600 °C, 800 °C, 1000 °C) to investigate optimal preparation conditions. The iron-phthalocyanine/C (PcFe/C) catalyst was prepared in the same method.

2.3. Bulk and surface analyses

XRD spectroscopy was performed with an automated Bruker Beijing Office, China D8 Advance Powder diffractometer. X-ray radiation was obtained using a long line of fine-focus copper tube powered at 800 W. The Kα radiation ($\lambda = 1.54178$Å) was isolated using a Nickel foil filter. Data acquisition was carried out in the $\theta/2\theta$ step scanning mode at a speed of 6° min^{-1} with a step size of 0.1° (2θ).

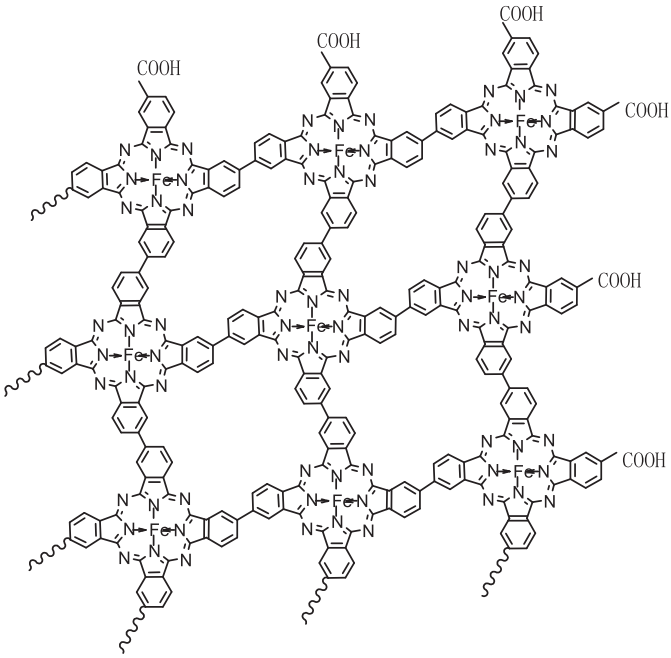

Fig. 2. The structure of PPcFe.

The surface of the PPcFe/C catalyst was characterized by XPS on a PHI-5300 ESCA spectrometer (Perkin Elmer Instruments, Waltham, MA).

2.4. Electrochemical measurements and durability test

The PPcFe/C catalysts were evaluated using the RDE (Perkin Elmer Instruments) technique and electrochemical setup consisting of an Electrochemical Workstation (CHI 660C; CH Instruments, Austin, TX) controlled by a computer. A total of 5 mg of finely ground catalyst were ultrasonically mixed for 1 h with 5 mL ultrapure water (18.23 MΩ cm^{-1}) and 0.05 mL 5wt % solution of perfluorinated ion-exchange resin (NafionT; DuPont de Nemours, Wilmington, DE). Subsequently, 6 μL catalyst ink was pipetted and spread onto a glassy carbon disk ($\Phi = 3.4$ mm), which was used as the rotating electrode. The film was dried in air at 75 °C. RDE measurements were performed in a three-electrode cell, where a Pt filament was used as the counter electrode and Hg/Hg_2SO_4 in saturated K_2SO_4 solution as the reference electrode [0.6151 V versus (vs.) SHE]. All potentials reported in this paper are relative to the RHE. The surface area of the working electrode was 0.1075 cm^2. Electrochemical measurements were carried out in 0.5 M L^{-1} H_2SO_4 solution saturated with oxygen (O_2) or Ar under quasi-stationary conditions at 20 °C at a sweep rate of 5 mV s^{-1}. The linear sweep voltammetry (LSV) was determined at different rotation speeds.

Durability experiments were carried out for the PPcFe/C catalysts using continuous and repeated cyclic voltammetry (CV), LSV, and chronoamperometry, with the electrode rotation rate fixed at 1500 rpm. Cyclic voltammograms were obtained after 30 min of equilibration between consecutive cycles. The resulting PPcFe was characterized by FTIR spectroscopy. The infrared (IR) spectra of the samples were recorded on a Nicolet 5700 spectrophotometer (ThermoFisher Scientific, Waltham, MA) using KBr pellets. The tests were performed between 4000 and 400 cm^{-1}. To compare the durability of PPcFe catalyst with a PcFe catalyst, we conducted a PcFe/C durability test by CV, LSV, and chronoamperometry in the same testing environment.

2.5. Preparation of air electrode

The air electrode consisted of a microporous gas diffusion layer, a porous nickel foam substrate as current collector, and a catalyst layer. The electrode area was 25 cm^2 (5 cm × 5 cm).

The gas diffusion layer is prepared as follows: Briefly, acetylene carbon black (Yiborui Chemical Industry Company, Tianjin, China) and poly-tetrafluoro-ethylene colloidal (PTFE; DuPont de Nemours, Wilmington, DE) were fully mixed in absolute ethanol in 1:1 weight proportion and then mixed with 33 wt% anhydrous sodium sulfate pore-former. The slurry was mixed ultrasonically for 2 h to form a homogeneous suspension and then dried at 75 °C to produce a dough-like paste. The paste was coated on one side of the porous nickel foam (Tianyu Technology Company, Heze, China) substrate as a current collector.

PPcFe/C, PcFe/C, and Pt/C air cathode catalysts were prepared for comparative testing. The loading of the FeN_4 active ORR sites was 1.0 mg cm^{-2}. The loading of the commercial E-TEK Pt/C catalyst (De Nora North America ETEK Division, Somerset, NJ: 30 wt % Pt on Vulcan XC-72 carbon black) was 1.0 mg cm^{-2} of Pt. The catalyst layer of the air electrode was prepared by mixing catalyzed carbon black (Vulcan XC-72), acetylene carbon black, and PTFE dispersed in ethanol in the mass proportions of 2:1:3. The slurry was dried at 75 °C to produce a dough-like paste, as described above. The catalyst paste was coated on the other side of the porous nickel foam substrate. The air electrode was finally pressed for 2 min under a pressure of 10 MPa and then sintered for 60 min at 350 °C.

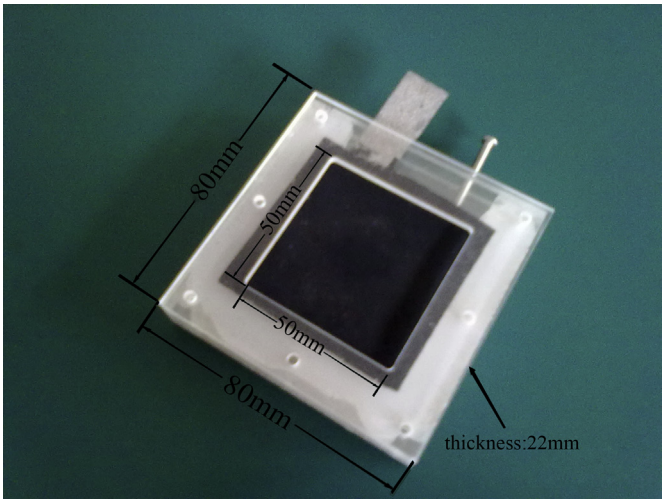

Fig. 3. The MAFC single cell.

The performances of the air electrode were evaluated using a CHI 660C Electrochemical Workstation.

2.6. The assembly of the MAFC single cells

Mg sheet (98.9% Mg, thickness: 8.5 mm, Changyu New Material Company, Shandong, China) was used as the anode. The air electrode is on one side of the Mg sheet. An in-house MAFC single cell insulating polymer case was used. The electrolyte is 10 wt% NaCl solution. The assembled MAFC single cell is shown in Fig. 3.

The discharge performance of the MAFC single cell was evaluated using an electronic load instrument (M9700, Maynuo Company, Nanjing, China).

3. Results and discussion

3.1. Ultraviolet–visible (UV–vis) and infrared (IR) analyses

The UV–vis absorption spectra of TcPcFe and PPcFe exhibited two typical strong absorption regions. The absorption bands of

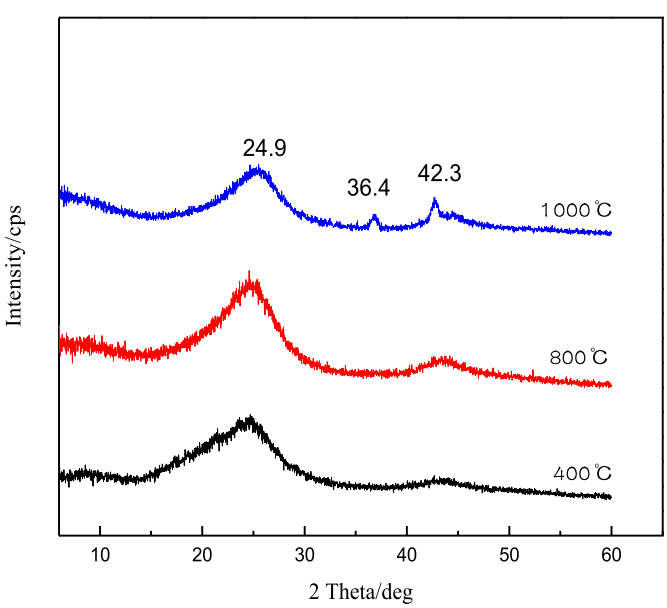

Fig. 4. XRD comparison of PPcFe/C heat-treated at different temperatures.

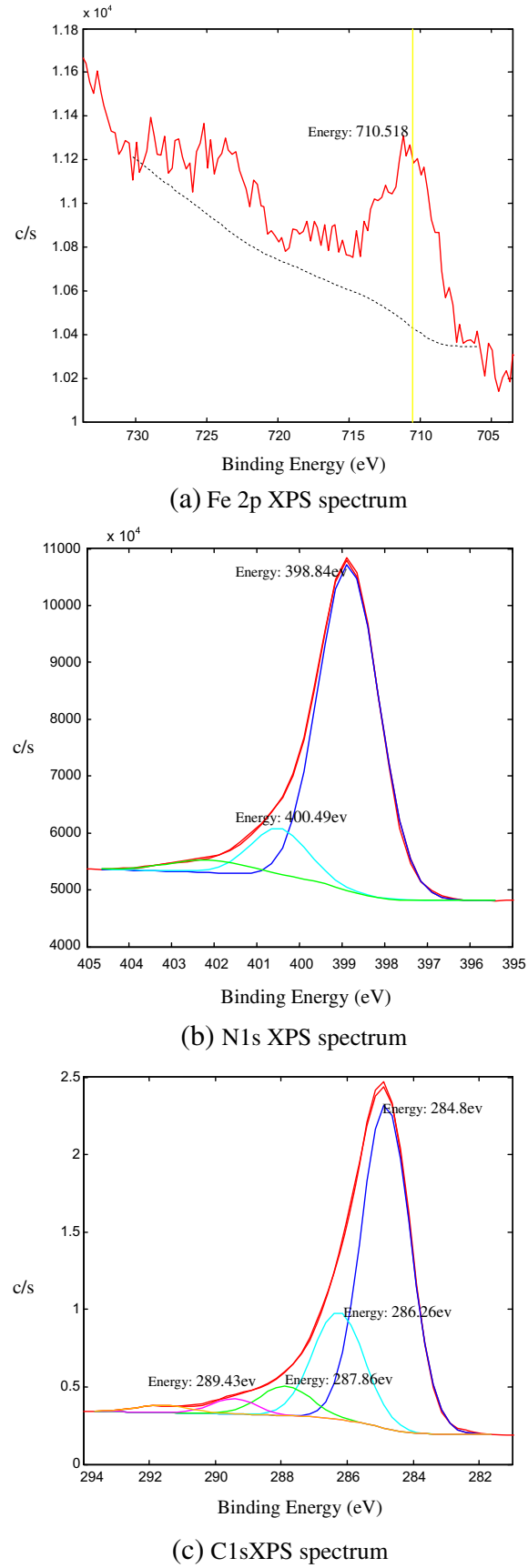

Fig. 5. XPS spectra of PPcFe/C (a) Fe 2p XPS spectrum (b) N1s XPS spectrum (c) C1s XPS spectrum.

PPcFe (315 nm) appeared at higher wavelengths than those of TcPcFe (302 nm). The red-shift in the peak supported the polymeric nature of the material [45].

The IR spectra of TcPcFe and PPcFe showed phthalocyanine skeletal absorption bands (749 cm^{-1}, 1090 cm^{-1}, 1716 cm^{-1}, 1751 cm^{-1}). The absorption peak of FeN_4 (907 cm^{-1}) was still observed. The decreased absorption peaks of the carboxylic acid groups (1599 cm^{-1}) were evidence of the polymerization reaction.

3.2. Bulk and surface analyses

The powder XRD analysis of PPcFe/C heated at different temperatures was performed over the 2θ angle range of 3°–60°. Fig. 4 shows that the XRD spectra of the PPcFe/C heated at 400 °C show no diffraction peak, only a diffuse reflection peak. The shape of the XRD spectrographs indicates that PPcFe is amorphous in nature. The PPcFe is well-dispersed on the surface of carbon black. The XRD patterns of PPcFe/C heated at 800 °C show that FeN_4 decomposed. A small amount of metal clusters also appeared. After heating at 1000 °C, crystalline products appear on the surface of the carbon black. Several α-Fe crystal diffraction peaks are observed at 36.4° and 42.3° 2θ range. Fe–N–C clusters are produced.

A thorough analysis of the composition and structure of PPcFe/C (400 °C, 1:1, FeN_4 loading of 7.5%) was conducted using XPS to determine the active center of the synthesized catalyst. Fig. 5(a)–(c) show the Fe 2p, N1s, and C1s regions of typical XPS spectra. The assignments of the peaks to certain species in this work are based on current and previous studies on the structure of metal phthalocyanines [46,47]. Fig. 5(a) shows that the binding energy bands at 710 eV of the Fe 2p XPS spectrum corresponded to Fe (II). The Fe atom was located at the ligand environment of the N-enriched structure of the phthalocyanine ring. N was found in several forms. Fig. 5(b) shows that the main peak at 398.84 eV of the N 1s spectra could be ascribed to the two chemically non-equivalent *N* atoms (four central *N* atoms in the pyrrole ring and four aza-bridging *N* atoms (–C=N–C=)) [48]. The latter peak at 400.49 eV could be attributed to a shake-up satellite [49]. Fig. 5(c) shows that the bands at 284.8, 286.26, 287.86, and 289.43 eV of the C1s spectra could respectively be attributed to the aromatic C–C bonds as well as N–C=N, C=O, and C=C bonds [50]. A shake-up satellite appeared at 291.59 eV. The XPS spectra suggest that the phthalocyanine ring in the catalysts was not destroyed, further confirming that the active site of the catalyst is the FeN_4 in the phthalocyanine ring.

3.3. Electrochemical study of ORR at PPcFe/C

In order to test the electrochemical activity of the PPcFe/C, the rotating disk electrode method was employed to investigate the diffusion kinetics of O_2 reduction. Fig. 6 shows the current–potential curves recorded using a rotating disk electrode, coated with PPcFe/C, at different rotation rates in an O_2-saturated 0.5 M L^{-1} H_2SO_4. The limiting currents can be observed when the electrode potential is moved to increasingly negative voltages, indicating that the diffusion process becomes the dominating step in the electrocatalytic reaction. Limiting currents were plotted against the square root of the rotation rate as in Fig. 6. A linear relationship was observed. The straight line obeys the Koutecky–Levich equation [51].

$$1/I = 1/I_K + 1/I_d = 1/I_K + 1/B\omega^{1/2} \quad (1)$$

$$I_d = c0.62nFACo_2\omega^{1/2}Do_2{}^{2/3}\gamma^{-1/6} \quad (2)$$

$$I_K = 10^3nFAK\tau \quad (3)$$

In these equations, *F* is Faraday's constant, *B* is *K–L* slope, *A* is the electrode area, *n* is the electron number involved in the ORR, Co_2 is the oxygen concentration, Do_2 is the oxygen diffusion coefficient in the medium, and ω the electrode rotation speed and *K* is the

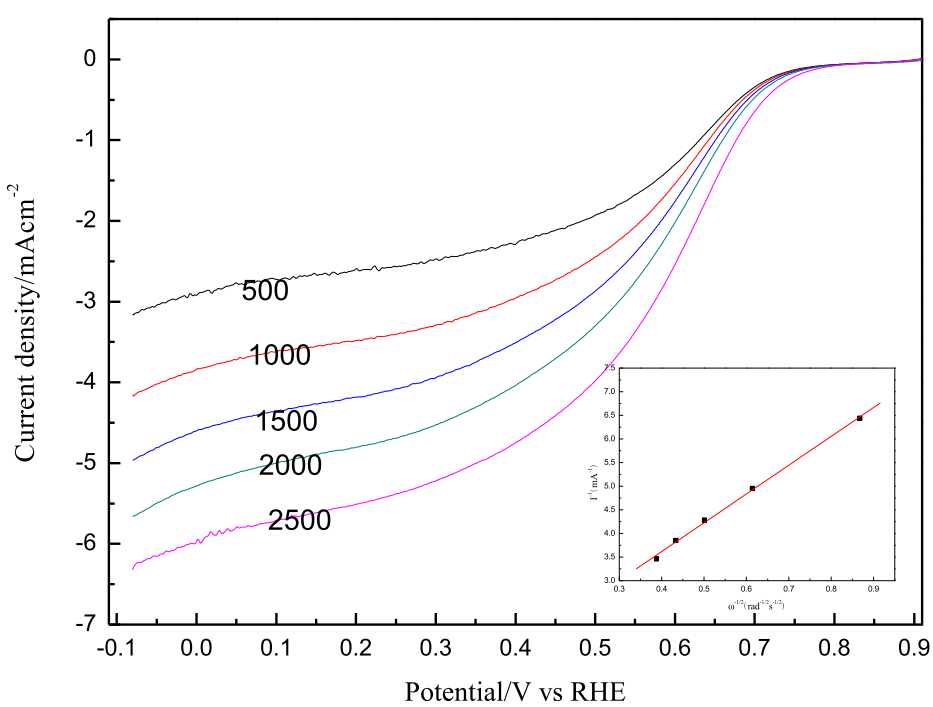

Fig. 6. Polarization cures at different rotation rates ω recorded at PPcFe/C electrode in O_2-saturated 0.5 M L^{-1} H_2SO_4 ($T = 20$ °C, Cv = 5 mV s^{-1}). Inset right: Koutecky–Levich plots determined from polarization cures at different rotation rates.

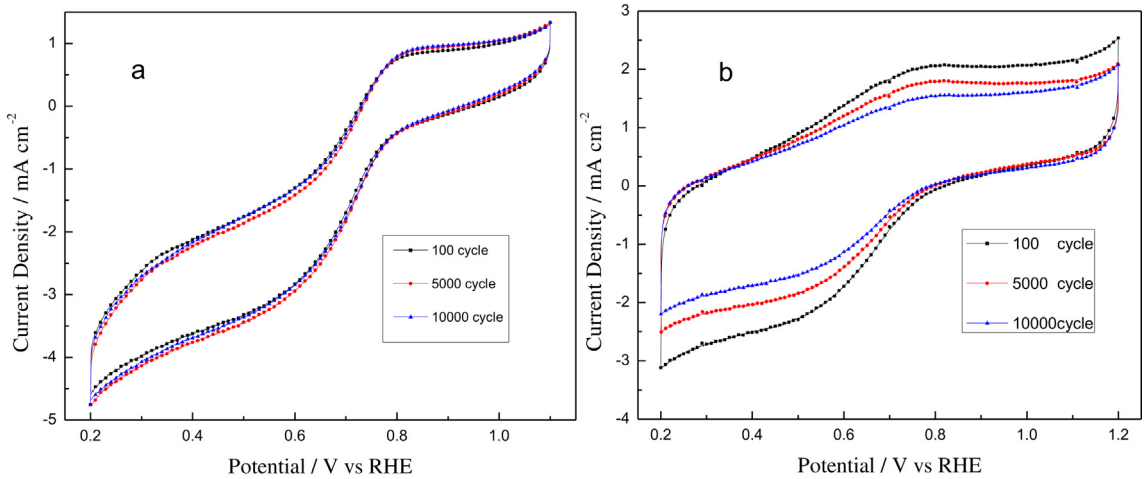

Fig. 7. Cyclic voltammetry curves (a) PPcFe/C; (b) PcFe/C; electrode in O_2-saturated 0.5 M L^{-1} H_2SO_4 (20 °C; 5 mV s^{-1}).

reaction rate constant, γ is the kinetic viscosity of the electrolyte solution, τ is the surface concentration.

The RDE result show the best loading is PPcFe:C = 1:1 (FeN_4 loading is 7.5%) and the best heat-treatment temperature is 400 °C. The onset potential of PPcFe/C catalysts for O_2 reduction is 0.82 V vs. RHE at 20 °C. The catalyst is prepared in this optimal technology and then the number of electrons transferred is obtained. Combining Eqs. (1)–(3) and using the slopes from Fig. 6, the number of electrons transferred, which gives $n = 3.83$, which is relative to the number of transferred electrons for Pt/C which is assumed to be 4.0.

3.4. Electrochemical measurements with spectroscopy durability test

Life stability experiments were performed using cyclic voltammogram (CV), chronoamperometry, and LSV methods in O_2-saturated H_2SO_4 to investigate whether the degradation results from the demetalation of PPcFe. The CVs are shown in Fig. 7. Fig. 7(a) shows no electrocatalytic activity loss after CV scanning at 10,000 cycles over 4 days. Fig. 7(b) shows that the performance of the PcFe catalyst was reduced by 0.8 mA cm^{-2} after 10,000 cycles.

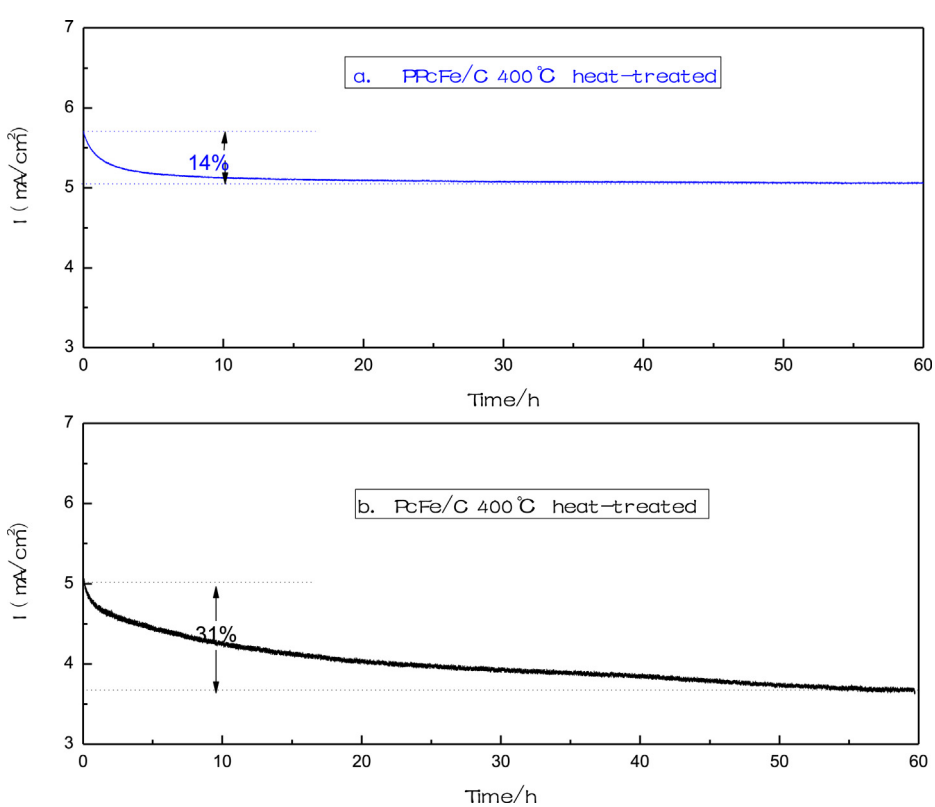

Fig. 8. Current density as a function of time recorded at (a) PPcFe/C (b) PcFe/C working conditions: O_2-saturated 0.5 M L^{-1} H_2SO_4 (20 °C; 0.5 V vs. RHE.).

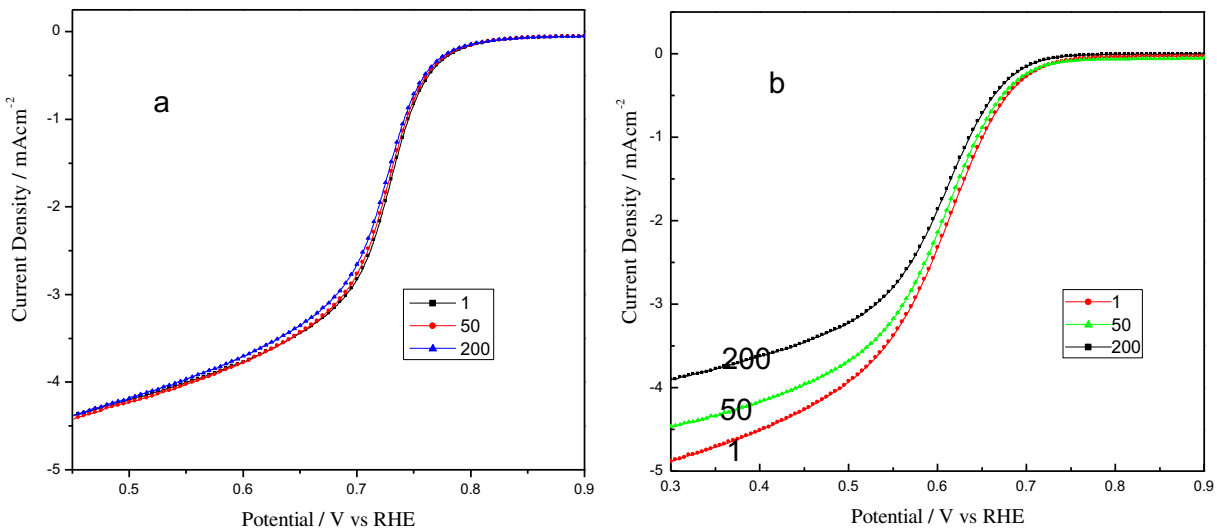

Fig. 9. Study of the electrode durability: polarization curves of the first 200 cycles for oxygen reduction on (a) PPcFe/C; (b) PcFe/C rotating disk electrode recorded at 1500 rpm in O_2-saturated 0.5 M L^{-1} H_2SO_4 electrolyte (20 °C; 5 mV s^{-1}).

Fig. 8 shows the chronoamperometry curve recorded at 0.5 V vs. RHE. The figure shows that the performance of PPcFe/C deteriorated by 14%, whereas that of PcFe/C degraded by 31%. Fig. 8(a) shows that the performance deterioration of PPcFe/C was not as severe as indicated by previous studies (i.e., the oxygen reduction current is about 65% lower than at the beginning of the measurements after 3 h) [52]. A durability test of PcFe/C was also performed under the same conditions to facilitate a comparison with PcFe/C. The results are shown in Fig. 8(b). The electrocatalysis decay of PcFe/C was evidently more serious than that of PPcFe/C.

Fig. 9 shows the polarization curves for the O_2 reduction on a PPcFe/C RDE. Fig. 9(a) shows that the O_2 reduction current was almost unchanged from cycle 1 to cycle 200. Fig. 9(b) shows that the O_2 reduction current for PcFe/C decreased drastically after long polarization test time.

After all electrochemical measurements (i.e., CV, LSV, and chronoamperometry), PPcFe/C was dispersed in dimethyl sulfoxide. After filtering the solution, dimethyl sulfoxide was evaporated, leaving pure PPcFe. The original PPcFe and extracted PPcFe were characterized by FT-IR analysis. The results are shown in Fig. 10. The figure shows that phthalocyanine skeletal absorption bands were still observed in the polymeric materials, indicating the presence of phthalocyanine structures. Thus, the FT-IR analysis indicates that PPcFe was not destroyed under electrochemical conditions in O_2-saturated acidic media. Three factors may have contributed to the significant durability of PPcFe/C. First, PPcFe don't decompose at

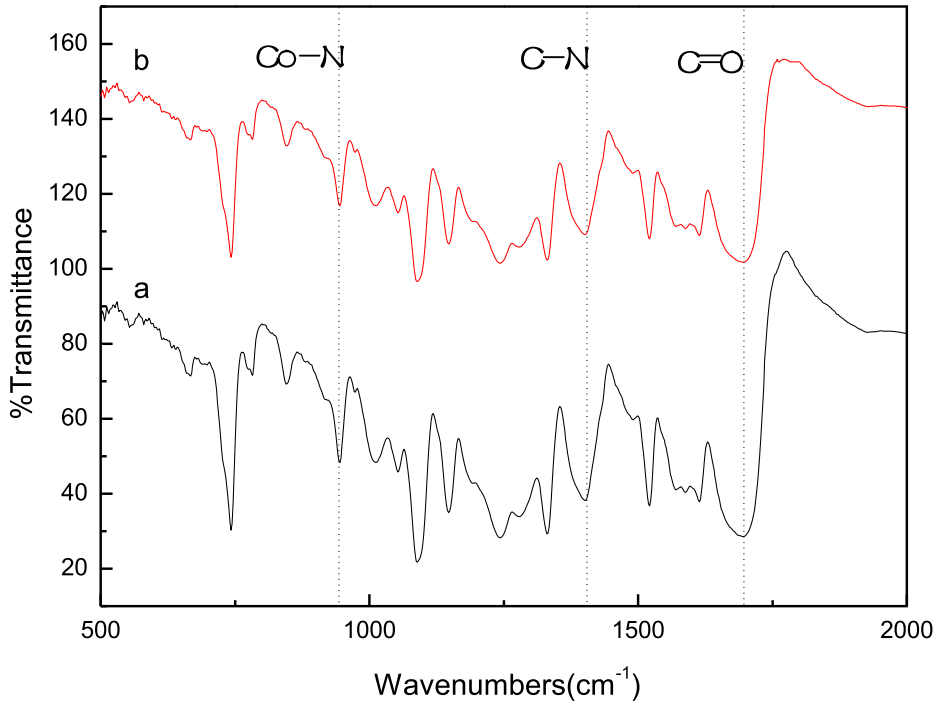

Fig. 10. FT-IR spectra of PPcFe (a) before and (b) after electrochemical measurement.

activation temperature of 400 °C. Thus, PPcFe did not decompose at 400 °C, thus has excellent chemical stability. In contrast, when PcFe/C is heated at 400 °C, the PcFe/C is partly converted to Fe–N–C clusters. During long testing times in acid medium, the Fe–N–C cluster is not stable and demetallation occurred, reducing the number of active sites per unit area, and giving catalytic performance decay. Second, for the monomer, all the atoms of Pc ring are in a plane, which form one molecular pi (π) bond. In PPcFe, PcFe rings are connected by single bonds in a planar array, so that a planar conjugated structure can form between the π orbitals from different Pc rings which can overlap to form a large-area pi (π) bond, giving a more stable structure. Third, anchoring of PPcFe to the carbon support appears to be tighter, primarily because of the effect of heat treatment.

3.5. Electrochemical properties of the air electrodes

The polarization curves are constructed to determine the electrochemical properties of the air electrode. The polarization curves of the air electrodes with different catalysts for O_2 reduction in 10 wt % NaCl are shown in Fig. 11. A saturated calomel (SCE) reference electrode was used (+0.2415 V vs. SHE). Linear polarization analyses were performed using a CHI 660C electrochemical system. The potential of air electrode loaded with commercial Pt/C, PPcFe/C, and PcFe/C catalyst is at a current density of 50 mA cm^{-2} is −0.014, −0.106, and −0.25 V versus RHE, respectively. The current densities of the air electrodes at a polarization potential of −0.400 V are 295.7, 238.0, and 107.6 mA cm^{-2}. These results indicate that Pt/C and PPcFe/C exhibit similar catalytic effects and that PPcFe/C has a distinct advantage over PcFe/C.

3.6. Performance of MAFCs

Discharge experiments were performed at different currents and constant currents to test the discharge performance of single MAFCs. The discharge curves of single MAFCs with different catalysts are shown in Fig. 12. The performances of single MAFCs with PPcFe/C and PcFe/C catalysts are similar at low current density. The performances of the two catalysts significantly differ from that of the Pt/C catalyst. The PPcFe/C catalyst is similar to the Pt/C catalyst and has an evident advantage over the PcFe/C catalyst at high

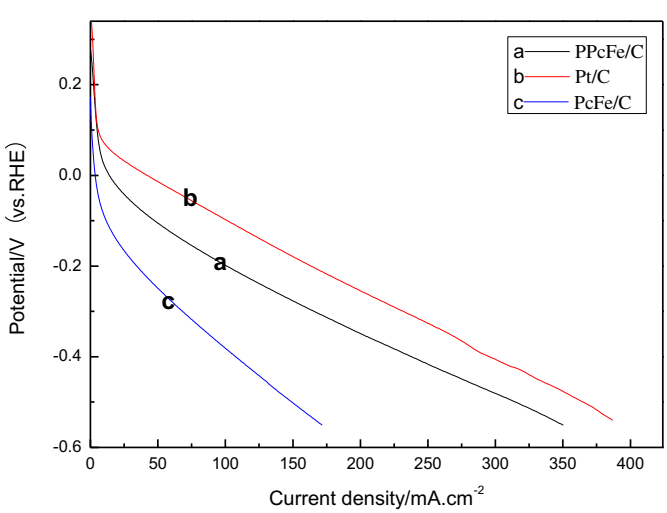

Fig. 11. The linear polarization curves of air cathode electrodes with different catalysts in 10 wt% NaCl at 20 °C. Scan rate: 20 mV s^{-1}; electrode area: 1 cm^2; Counter electrode: nickel sheet; reference electrode: saturated calomel electrode (SCE, +0.2415 V vs. SHE).

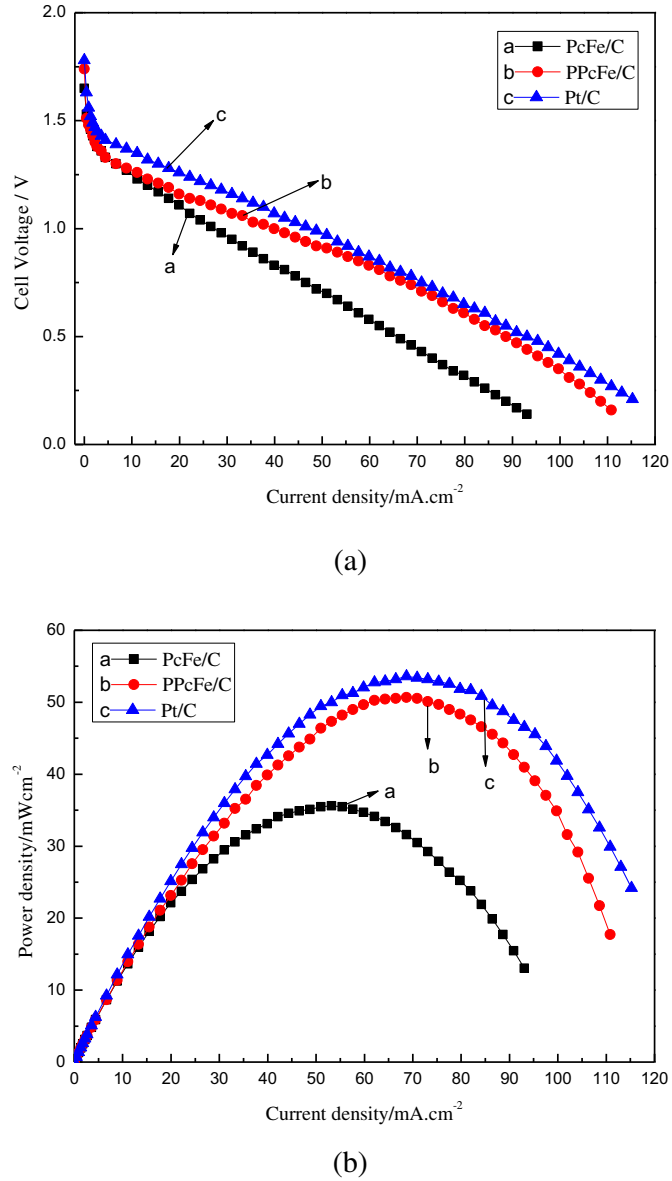

Fig. 12. Discharge performances of magnesium–air fuel cells with different cathode catalysts. Temperature: 20 °C; anode: 98.9% magnesium; electrolyte: 10 wt% NaCl solution.

current density. Fig. 12(a) shows that the cell voltage of a MAFC using a PPcFe/C catalyst was 0.83 V at a current density of 60 mA cm^{-2}, which is close to that of MAFC using a Pt/C catalyst, which is 0.87 V Fig. 12(b) shows that the peak power densities of the MAFC using PPcFe/C, PcFe/C, and Pt/C catalysts are 50.5, 35.5, and 53.2 mW cm^{-2}, respectively.

PPcFe/C catalyst shows excellent ORR activity. In terms of the molecular orbital theory, PPcFe may have a less localized π bond and a higher delocalization energy than those of the monomer, resulting in a smaller HOMO-LUMO gap. This may explain why PPcFe will more easily receive and donate electrons and show greater activity and selectivity.

Fig. 13 shows the discharge curves of single MAFCs with different catalysts at constant current density of 20 mA cm^{-2} over 11 h. Single MAFCs show excellent stability over the entire test duration. The working voltage of the MAFC with PPcFe/C catalyst was eventually approximately 100 mV higher than that of the cell with PcFe/C catalyst. The difference in the discharge curves

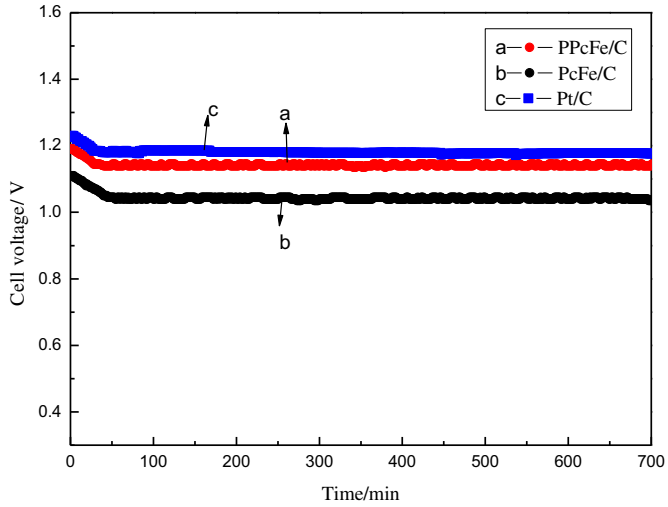

Fig. 13. The discharge curves of the magnesium–air fuel cells with different cathode catalysts at constant current of 20 mA cm^{-2}; Temperature: 20 °C; anode: 98.9% magnesium; electrolyte: 10 wt% NaCl solution.

indicates that the cell using PPcFe/C catalyst exhibited better discharge characteristics than that using the PcFe/C catalyst. These results show that an MAFC cathode using PPcFe/C catalyst has an ORR catalytic activity close to one using Pt/C, which is significantly higher than that using PcFe/C catalyst.

4. Conclusion

The PPcFe/C catalyst used for an air electrode in unbuffered 10 wt % NaCl electrolyte (i.e., in more alkaline solution under load) is inexpensive and easy to prepare. XRD analysis indicates that PPcFe/C is amorphous when heated at 400 °C. XPS analysis indicates that the active site of the PPcFe/C catalysts is FeN_4 in the phthalocyanine ring. The onset potential of the PPcFe/C catalysts for O_2 reduction in O_2-saturated H_2SO_4 is 0.82 V vs. RHE at 20 °C. PPcFe/C catalyzes O_2 reduction mainly through a four-electron process. Electrochemical and FTIR testing showed that PPcFe/C catalyst exhibits excellent durability and electrochemical properties. The ORR catalysis of MAFC single cells using PPcFe/C has an evident advantage over those with PcFe/C, and they show similar performance to those with Pt/C catalyst at high current densities. MAFC single cells with PPcFe/C catalysts have been shown to operate uninterruptedly for more than 11 h with a decrease in cell voltage of less than 0.01 V.

Acknowledgments

This work was financially supported by the National Natural Science Foundation of China (grant nos. 21276148, 21076119, and 20776081) and the Natural Science Foundation of Shandong Province, China (grant no. ZR2010BM004 and Y2006B37)

References

[1] F.Y. Cheng, J. Chen, Chem. Soc. Rev. 41 (2012) 2172–2192.
[2] R.G. Cao, J.S. Lee, M.L. Liu, J. Cho, Adv. Energy Mater. 2 (2012) 816–829.
[3] W.Q. Yang, S.H. Yang, J.S. Guo, G.Q. Sun, Q. Xin, Carbon 45 (2007) 397–401.
[4] J.S. Lee, T. Lee, H.K. Song, J. Cho, B.S. Kim, Energy Environ. Sci. 4 (2011) 4148–4154.
[5] S.H. Yang, H. Knickle, J. Power Sources 112 (2002) 162–173.
[6] Y.L. Li, J.J. Wang, X.F. Li, J. Liu, D.S. Geng, J.L. Yang, R.Y. Li, X.L. Sun, Electrochem. Commun. 13 (2011) 668–672.
[7] J.O. Besenhard, M. Winter, Chem. Phys. Chem. 3 (2002) 155–159.
[8] B.C.H. Steele, A. Heinzel, Nature 414 (2001) 345–352.
[9] Y. Wang, K.S. Chen, J. Mishler, S.C. Cho, X.C. Adroher, Appl. Energy 88 (2011) 981–1007.
[10] W. Vielstich, A. Lamm, H.A. Gasteiger, Handbook of Fuel Cell-fundamentals, Technology and Applications, Wiley, Chichester, 2003.
[11] X.M. Ma, H. Meng, M. Cai, P.K. Shen, J. Am. Chem. Soc. 134 (2012) 1954–1957.
[12] D. Banham, F. Feng, K. Pei, S. Ye, V. Birss, J. Mater. Chem. A1 (2013) 2812–2820.
[13] M. Wang, W. Zhang, J. Wang, A. Minett, V. Lo, H. Liu, J. Chen, J. Mater. Chem. A1 (2013) 2391–2394.
[14] M.J. Liao, Z.D. Wei, S.G. Chen, L. Li, M.B. Ji, Y.Q. Wang, Int. J. Hydrogen Energy 35 (2010) 8071–8079.
[15] Z.W. Chen, D. Higgins, A.P. Yu, L. Zhang, J.J. Zhang, Energy Environ. Sci. 4 (2011) 3167–3192.
[16] L.Q. Mao, D. Zhang, T. Sotomura, K. Nakatsu, N. Koshiba, T. Ohsaka, Electrochim. Acta 48 (2003) 1015–1021.
[17] Z. Lin, L.W. Ji, M.D. Woodroof, X.W. Zhang, J. Power Sources 15 (2010) 5025–5031.
[18] Y. Liu, A. Ishihara, S. Mitsushima, N. Kamiya, K. Ota, J. Electrochem. Soc. 154 (2007) B664–B669.
[19] X.M. Ren, S.S. Zhang, D.T. Tran, J. Read, J. Mater. Chem. 21 (2011) 10118–10125.
[20] C. He, Z. Li, M.L. Cai, M. Cai, J. Wang, Z. Tian, X. Zhang, P.K. Shen, J. Mater. Chem. A1 (2013) 1401–1406.
[21] Y. Zhao, K. Watanabe, K. Hashimoto, J. Mater. Chem. A1 (2013) 1450–1456.
[22] M. Lefèvre, E. Proietti, F. Jaouen, J.P. Dodelet, Science 324 (2009) 71–74.
[23] M.K. Song, S. Park, F.M. Alamgir, J. Cho, M. Liu, Mater. Sci. Eng. R 72 (2011) 203–252.
[24] J. Liang, Y. Jiao, M. Jaroniec, S. Qiao, Angew. Chem. Int. Ed. 51 (2012) 11496–11500.
[25] Y. Tang, B.L. Allen, D.R. Kauffman, A. Star, J. Am. Chem. Soc. 131 (2009) 13200–13201.
[26] K. Gong, F. Du, Z. Xia, M. Durstock, L. Dai, Science 323 (2009) 760–764.
[27] D. Geng, H. Liu, Y. Chen, R. Li, X. Sun, S. Ye, S. Knights, J. Power Sources 196 (2011) 1795–1801.
[28] R. Bashyam, P. Zelenay, Nature 443 (2006) 63–66.
[29] G. Wu, K.L. More, C.M. Johnston, P. Zelenay, Science 332 (2011) 443–447.
[30] S. Pylypenko, S. Mukherjee, T.S. Olson, P. Atanassov, Electrochim. Acta 53 (2008) 7875–7883.
[31] A. Okunola, B. Kowalewsk, M. Bron, P.J. Kulesza, W. Schuhmann, Electrochim. Acta 54 (2009) 1954–1960.
[32] V. Neburchilov, H. Wang, J.J. Martin, W. Qu, M. Liu, J. Power Sources 195 (2010) 1271–1291.
[33] Q.G. He, T. Mugadza, X.W. Kang, X.B. Zhu, S.W. Chen, J. Kerr, T. Nyokong, J. Power Sources 216 (2012) 67–75.
[34] W.M. Li, A.P. Yu, D. Higgins, B.G. Llanos, Z.W. Chen, J. Am. Chem. 132 (2010) 17056–17058.
[35] X.M. Hu, D.G. Xia, L. Zhang, J.J. Zhang, J. Power Sources 231 (2013) 91–96.
[36] R. Jasinski, Nature 201 (1964) 1212–1213.
[37] R. Baker, D.P. Wilkinson, J.J. Zhang, Electrochim. Acta 53 (2008) 6906–6919.
[38] Y.H. Lu, R.G. Reddy, Int. J. Hydrogen Energy 33 (2008) 3930–3937.
[39] Y.F. Ji, Z.F. Li, S.W. Wang, G.F. Xu, X.J. Yu, Int. J. Hydrogen Energy 35 (2010) 8117–8121.
[40] G.F. Xu, Z.F. Li, S.W. Wang, X.J. Yu, J. Power Sources 195 (2010) 4731–4735.
[41] Y. Lu, R.G. Reddy, Electrochim. Acta 52 (2007) 2562–2569.
[42] M. Ladouceur, G. Lalande, D. Guay, J.P. Dodelet, J. Electrochem. Soc. 140 (1993) 1974–1981.
[43] V.S. Bagotzky, M.R. Tarasevich, K.A. Radyushkina, O.A. Levina, S.I. Andrusyova, J. Power Sources 2 (1998) 233–240.
[44] B.N. Achar, et al., U S. Patent, 1984, No. 4450268.
[45] B.N. Achar, K.S. Lokesh, J. Organ. Chem. 689 (2004) 2601–2605.
[46] F. Jaouen, F. Charreteur, J.P. Dodelet, J. Electrochem. Soc. 153 (2006) A689–A698.
[47] A.L. Bouwkamp-Wijnoltz, W. Visscher, J.A.R. Van Veen, Electrochim. Acta 43 (1998) 3141–3152.
[48] H. Hochst, A. Goldmann, S. Hufner, H. Malter, Phys. Status Solidi B Basic Res. 76 (1976) 559–568.
[49] P. Garcia, J.F. Espinal, C.S.M. de Lecea, F. Mondragon, Carbon 42 (2004) 1507–1515.
[50] G. Beamson, D. Briggs, High Resolution XPS of Organic Polymers: the Scientia ESCA300 Database, John Wiley & Sons, Chichester, 1992, pp. 277–282.
[51] A.J. Bard, L.R. Faulkner, Fundamental Sand Applications, Wiley, New York, 1980.
[52] S. Baranton, C. Coutanceau, C. Roux, F. Hahn, J.M. Leger, J. Electroanal. Chem. 577 (2005) 223–234.